Journal of Applied Physics ARTICLE pubs.aip.org/aip/jap

Characterization and optimization of high-efficiency crystalline silicon solar cells: Impact of recombination in the space charge region and trap-assisted Auger exciton recombination

Cite as: J. Appl. Phys. **137**, 023101 (2025); doi: 10.1063/5.0239369
Submitted: 19 September 2024 · Accepted: 20 December 2024 ·
Published Online: 9 January 2025

V. P. Kostylyov,[1,a)] A. V. Sachenko,[1] M. Evstigneev,[2] I. O. Sokolovskyi,[1] and A. I. Shkrebtii[3]

AFFILIATIONS

[1]V. Lashkaryov Institute of Semiconductor Physics, NAS of Ukraine, 41 prospect Nauky, 03028 Kyiv, Ukraine
[2]Department of Physics and Physical Oceanography, Memorial University of Newfoundland, St. John's, Newfoundland and Labrador A1B 3X7, Canada
[3]Faculty of Science, Ontario Tech University, 2000 Simcoe Street North, Oshawa, Ontario L1G 0C5, Canada

[a)]**Author to whom correspondence should be addressed:** vkost@isp.kiev.ua

ABSTRACT

Since the photoconversion efficiency η of the silicon-based solar cells (SCs) under laboratory conditions is approaching the theoretical fundamental limit, further improvement of their performance requires theoretical modeling and/or numerical simulation to optimize the SCs parameters and design. The existing numerical approaches to modeling and optimizing the key parameters of high-efficiency solar cells based on monocrystalline silicon, the dominant material in photovoltaics, are described. It is shown that, in addition to the four usually considered recombination processes, namely, Shockley–Read-Hall, surface, radiative, and band-to-band Auger recombination mechanisms, the non-radiative exciton Auger recombination and recombination in the space charge region (SCR) have to be included. To develop the analytical SC characterization formalism, we proposed a simple expression to model the wavelength-dependent external quantum efficiency of the photocurrent near the absorption edge. Based on this parameterization, the theory developed allows for calculating and optimizing the base thickness-dependent short-circuit current, the open-circuit voltage, and the SC photoconversion efficiency. The accuracy of the approach to optimizing solar cell parameters, particularly thickness and base doping level, is demonstrated by its application to three Si solar cells reported in the literature: one with an efficiency of 26.63%, another with 26.81%, and a third with a record efficiency of 27.3%. The results show that the developed formalism enables further optimization of solar cell thickness and doping levels, leading to potential increases in efficiency.

I. INTRODUCTION

Enormous progress has been achieved in photovoltaics (PV) since the invention of the first practical silicon solar cell (SC), as published 70 years ago.[1] This breaking applied research has initiated a new field of photovoltaic solar energy conversion and transformed it into a major component of the renewable energy sector. More than 60 years ago, Shockley and Queisser in their paper[2] laid the theoretical foundations for the fundamentals of solar cell operation and related photoconversion efficiency η, see also Refs. 3, 4, 5, and 6. After the research by Shockley and Quiesser,[2] the theoretical limit of photoconversion efficiency under the AM1.5G irradiation conditions for single-junction Si SCs has been extensively studied by numerous groups,[7–16] all reporting the values around 29.5 % up to a few tenths of a percent.

Even though various strategies to overcome this limit in photovoltaics have been proposed (see, e.g., Ref. 17 and references therein), crystalline silicon (c-Si) based SCs remain the most practical, cost-effective, stable, and durable component for the

photoconversion of solar energy into electricity for terrestrial applications. Si-wafer based PV technology accounted for about 97% of the total world production in 2023. Mono-crystalline technology became the dominant technology in c-Si production. As a result, the past two decades have witnessed a remarkable surge in silicon solar cells' efficiency in laboratory[18] and industrial[19] settings. Notably, researchers and technologists at LONGi have achieved significant milestone by developing a large-area SC sample with a record-breaking photoconversion efficiency of 26.81%,[20] surpassing the previous record of 26.7%[21,22] by 0.1%. This achievement underscores the formidable challenge of further enhancing photoconversion efficiency and suggests that we are approaching the practical limit for silicon SCs with either homo- or heterojunctions. Furthermore, the LONGi group has very recently reported a further whopping efficiency increase to 27.3%.[20]

The technological advancements can be attributed primarily to the improved methods of material growth and manufacturing of low-defect, low-contamination wafers, with photoexcited carrier lifetimes of the order of tens of milliseconds. Additionally, there have been significant developments in effective surface passivation techniques and interface engineering.[23–29] These developments have led to a notable increase in the measured effective lifetime of charge carriers, while simultaneously reducing the contribution of removable (extrinsic) recombination mechanisms compared to non-removable (intrinsic) ones. This trend is supported by recent research focusing on refining the parameterization of the intrinsic Auger and radiative recombination mechanisms,[13,14,30] which further highlights the critical importance of the accurate description of intrinsic recombination in silicon SCs close to the theoretical efficiency limit. As efforts in improving manufacturing processes and exploring new generation solar cell concepts, such as polysilicon on oxide (POLO)[31]/tunnel oxide passivating contacts (TOPCon),[32] continue to evolve, the emphasis on understanding and mitigating the recombination mechanisms in silicon will undoubtedly persist.

The necessity for an accurate description of intrinsic recombination in silicon arises from a broader requirement for the precise characterization of all recombination channels affecting non-equilibrium (excess) charge carriers, both intrinsic and extrinsic, within crystalline silicon-based solar cells. To address this challenge, the development of theoretical principles for the comprehensive characterization of silicon SCs and their practical application becomes essential.

Currently, many tools have been developed to perform SC modeling.[4,33–35] These tools and software products have shown their effectiveness in modeling and optimizing single-junction silicon SCs with homo- and heterojunction.[35–38] However, their common limitations are that they all consider four principal recombination mechanisms in silicon: Shockley–Read–Hall (SRH) recombination, Auger recombination, radiative recombination, and surface recombination. This paper presents an argument that two additional recombination channels need to be included to correctly describe the dependence of the effective lifetime on the excess concentration of charge carriers and the SC output power on the applied voltage: they are recombination in the space charge region (SCR, Fig. 1) and the trap-assisted Auger exciton recombination (Fig. 2). Exciton recombination can occur through two channels:

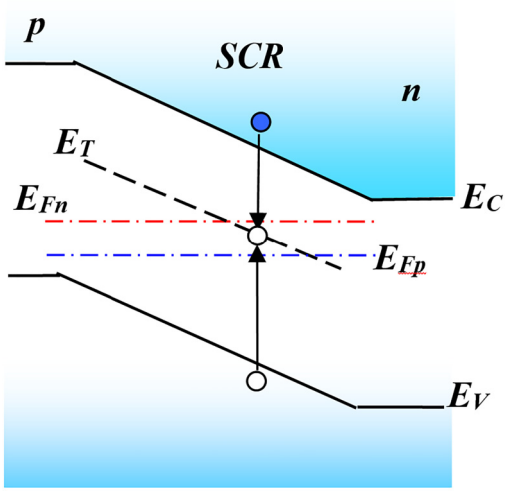

FIG. 1. Schematic illustration of the electron–hole pair recombination in the space charge region (SCR).

either as a result of the radiative recombination of an electron and a hole in an exciton, which is commonly called exciton annihilation, or in a non-radiative way involving the Auger mechanism via deep center.[39–43] In particular, it can occur due to the interaction of an exciton with a local center, as a result of which the exciton disappears, and a hot charge carrier, an electron or a hole, respectively, is emitted into the conduction band or into the valence band according to the Auger mechanism (Fig. 2).

The latter exciton recombination mechanism[39–41] appears because the spatial localization of an electron and a hole in an exciton significantly increases the probability of the Auger recombination. In such a process, either an electron or a hole is captured by the trap, while the energy and momentum released are carried away by the other quasi-particle that forms an exciton. This recombination process acts in parallel with the SRH recombination; as a result, the effective carrier lifetime is shorter than the "pure" SRH lifetime by a factor that increases with the doping level.[42,43]

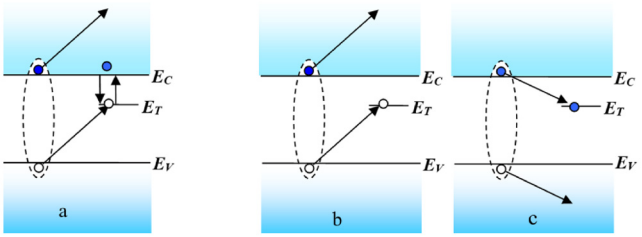

FIG. 2. Schematic illustration of the non-radiative trap-assisted Auger exciton recombination[39–43] in the case of a moderate (a) and high excitation level [(b) hole capture and (c) electron capture].

The next feature of our approach is the use of a simple analytical formula[44] to simulate the dependence of the external quantum efficiency on the wavelength and SC thickness near the absorption edge. Although this formula contains only one fit parameter, its comparison with the experimental curves of the short-circuit current and the photoconversion efficiency vs cell thickness showed excellent agreement.[44,45]

To enhance the parameters of next-generation silicon SCs, especially aiming for increased efficiency, a meticulous characterization of these cells stands as a primary requisite. The results reported in our study elucidate that employing six rather than four recombination processes, notably incorporating the recombination rate in the SCR, offers a more comprehensive SC characterization compared to the prevalent practice of utilizing four recombination processes. Our research underscores a crucial finding: it is the recombination within the SCR, rather than surface recombination, which predominantly is responsible for the diminished value of the effective lifetime of nearly all silicon SCs with well-passivated surfaces. Thus, prioritizing the investigation of its impact on the attributes of highly efficient silicon SCs is imperative.

II. EXTERNAL QUANTUM EFFICIENCY AND SHORT CIRCUIT CURRENT DENSITY

The external quantum efficiency, $EQE(\lambda)$, allows finding the short-circuit current density given the spectral density of the incident photon flux $I(\lambda)$ as

$$J_{SC} = q \int d\lambda \, EQE(\lambda) \, I(\lambda), \tag{1}$$

where q is the elementary charge. In the actual SCs, the $EQE(\lambda)$ dependence is determined by such factors as the chemical composition and morphology of the surface, the presence of a coating with a TCO (Transparent Conductive Oxide) layer or a grid for the current collection, the absorption coefficient of the semiconductor, and other factors.

However, the external quantum efficiency $EQE(\lambda)$ can be modeled with an analytical expression that involves several fit parameters.[38,46] We will be using a simpler alternative expression that gives this function for SCs of arbitrary base thickness and uses just two fit parameters.[44] These parameters are determined from a single experimental $EQE(\lambda)$ curve measured for one particular thickness. The idea behind this approach is as follows.

The wavelength-dependent external quantum efficiency curve can be divided into two regions: the short-wavelength region $\lambda < 800$ nm, which is denoted by the index s, in which the external quantum efficiency practically does not depend on the SC thickness d, and the long-wavelength region $\lambda > 800$ nm, denoted by the index l, in which the thickness dependence is present. Thus, this characteristic wavelength is defined by the condition that it separates the regions in which the EQE value depends on the SC thickness from those where it does not. This value must be determined separately for each case, but for the examples considered, it is the same for all SCs and is approximately 800 nm with sufficient accuracy. In the long-wavelength region, the fit expression is

$$EQE_l(\lambda) = \frac{f}{1 + b\,/(4n_r^2(\lambda)\,\alpha(\lambda)\,d)}, \tag{2}$$

where the fit parameter b determines the shape of the curve $EQE_l(\lambda)$ and the parameter f is chosen so as to match the values of EQE_s and EQE_l at $\lambda = 800$ nm. The non-dimensional parameter b has the physical meaning of the ratio of the photon mean path length $4n_r^2 d$ in an SC with ideal Lambertian surfaces to its actual mean photon path length. It depends on the surface texturing and the base thickness. For an ideally diffusive surface, this parameter has the value $b = 1$. Note that for the special choice $f = b = 1$, the expression (2) turns into the well-known absorptance formula.[7]

In the short-wavelength region $\lambda < 800$ nm, the experimental $EQE_s(\lambda)$ curves do not depend on the thickness, but are determined only by the losses due to reflection, shading, and absorption of light outside the SC base region. The digitized $EQE_s(\lambda)$ curve obtained for one particular thickness is assumed to apply to samples of any thickness.

III. LIFETIME OF THE PHOTOEXCITED CARRIERS IN SILICON

The total lifetime of the photoexcited carriers in silicon SCs is defined by the intrinsic and extrinsic recombination mechanisms,

$$\tau_{eff}^{-1} = \tau_{intr}^{-1} + \tau_{extr}^{-1}, \tag{3}$$

where the intrinsic lifetime is formed by the radiative and Auger contributions,

$$\tau_{intr}^{-1} = \tau_r^{-1} + \tau_A^{-1}. \tag{4}$$

The extrinsic lifetime

$$\tau_{extr}^{-1} = \tau_{SRH}^{-1} + \tau_S^{-1} + \tau_{exc}^{-1} + \tau_{SCR}^{-1} \tag{5}$$

is formed by the Shockley–Read–Hall and surface recombination mechanisms (the first two terms in the above expression), as well as the exciton trap-assisted Auger and space charge region recombination channels (the third and the fourth terms). We note that in the majority of the existing approaches, the last two recombination channels are usually left out.

The non-radiative exciton Auger recombination mediated by a deep recombination level was first observed by Fossum.[47] Its model was developed later by Hangleiter,[39,40] who related the relevant lifetime to the SRH lifetime and the doping level n_0 as

$$\tau_{exc} = \tau_{SRH} \frac{n_x}{n_0}, \tag{6}$$

where the characteristic concentration was originally assigned a value $n_x = 7.1 \times 10^{15}\ \mathrm{cm}^{-3}$. This value was later refined[42] to $8.2 \times 10^{15}\ \mathrm{cm}^{-3}$ after analyzing a number of experimental works, in which the existence of this recombination mechanism is

confirmed. This mechanism is also described in detail in the monograph[48] and in the second appendix of the recent paper.[43]

We note that, in fact, it is not the SRH lifetime that is determined from the experiment, but the effective lifetime

$$\tau_{SRH,eff} = \frac{\tau_{SRH}}{1 + n_0/n_x}. \tag{7}$$

The experimentally determined effective SRH lifetime is always shorter than the "bare" SRH lifetime; the difference between the two increases with the level of base doping.

As for the recombination in the SCR, it will be shown below that without taking it into account, theoretical agreement with the experiment cannot be obtained for a number of characteristics of silicon SCs, especially for illuminated $I-V$ curves and for the relation between the SC output power and the applied voltage, as well as for the effective lifetime vs the excess concentration curves.

The radiative lifetime is given by the expression[10]

$$\tau_r^{-1} = B(1 - P_{PR})(n_0 + \Delta n), \tag{8}$$

where P_{PR} is the probability of photon recycling and B is the radiative recombination coefficient given by[49]

$$\begin{aligned} B &= \int_0^\infty dE\, B(E), \\ B(E) &= \tfrac{8\pi}{h^3}\, \alpha_{bb}(E) \left(\tfrac{n_r(E)\, E}{c_0\, n_{i,eff}}\right)^2 e^{-E/kT}. \end{aligned} \tag{9}$$

Here, c_0 is the speed of light in vacuum, h is Planck's constant, $n_r(E)$ is the refractive index, and $\alpha_{bb}(E)$ is the absorption coefficient for the photons of energy E that result in creation of an electron–hole pair, and

$$n_{i,eff}(V) = n_i\, e^{\Delta E_g(V)/(2kT)} \tag{10}$$

is the effective intrinsic concentration corrected with respect to the bandgap narrowing effect by the amount ΔE_g.[50] The photon recycling probability is given by

$$P_{PR} = B^{-1} \int_0^\infty dE\, B(E)\, A_{bb}(E), \tag{11}$$

where the absorptance is

$$A_{bb} = \frac{\alpha_{bb}}{\alpha_{bb} + \alpha_{FCA} + b/(4n_r^2 d)}. \tag{12}$$

The second term in the denominator is the coefficient of absorption by the free charge carriers.[51] This expression differs from the Tiedje–Yablonovich formula[7] by the parameter $b > 1$.

The Auger recombination time is given by the general expression

$$\tau_{Auger} = \frac{\Delta n}{C_e g_e \left(n^2 p - n_0^2 p_0\right) + C_h g_h \left(n p^2 - n_0 p_0^2\right)}, \tag{13}$$

where n and p are the electron and hole concentrations, n_0 and p_0 are their respective values in thermal equilibrium, $C_{e,h}$ are the Auger coefficients, and the non-dimensional factors $g_{e,h}$ account for the enhancement of the Auger process due to the Coulomb screening. Several expressions have been proposed for these parameters.[13,14,52] They will be compared in the context of the SC modeling as follows.

The SRH lifetime depends on the doping and excitation level in an n-type semiconductor as

$$\tau_{SRH} = \frac{\tau_{p0}(n_0 + n_1 + \Delta n) + \tau_{n0}(p_1 + \Delta n)}{n_0 + \Delta n}, \tag{14}$$

where the characteristic times $\tau_{p0} = 1/(V_p \sigma_p N_t)$ and $\tau_{n0} = 1/(V_n \sigma_n N_t)$ depend on the hole and electron thermal velocities, V_p and V_n, and the respective capture cross sections, σ_p and σ_n, by a trap of concentration N_t and energy E_t. Finally, the concentrations n_1 and p_1 are the electron and hole concentrations when $E_F = E_t$. Depending on the excess concentration Δn of the electron–hole pairs, the SRH lifetime changes between the low-injection and the high-injection extreme values.

The non-radiative exciton Auger lifetime is[42]

$$\tau_{exc} = \tau_{SRH}\, \frac{n_x}{n_0 + \Delta n}. \tag{15}$$

The surface recombination lifetime is

$$\tau_S = d/S, \tag{16}$$

where S is the net recombination velocity on the front and the rear surface. It depends on the doping and excitation levels according to

$$S = S_0 \left(\frac{n_0}{n_p}\right)^m \left(1 + \frac{\Delta n}{n_0}\right)^r. \tag{17}$$

In this expression, $S_0(n_0/n_P)^m$ is the surface recombination velocity at a low excitation level, n_p is the doping level at which $S = S_0$ for $\Delta n = 0$, and the exponents m and r are both of the order of 1.

Similarly, the SCR recombination time is related to the respective recombination velocity by

$$\tau_{SCR} = d/S_{SCR}. \tag{18}$$

In unprocessed silicon wafers intended for SC fabrication and used in the experimental measurements of the lifetime, the $\tau_{eff}(\Delta n)$ curves are known to saturate[52] at $\Delta n < 10^{15}\,\mathrm{cm}^{-3}$, whereas the effective lifetime in Si SCs has a maximum at some excess carrier concentration.[19,32] This difference can be attributed to the fact that in the c-Si samples used for the measurements, there is no p–n junction, hence the band bending on both surfaces of the Si-wafer is symmetrical and slightly depleting. In this case, SCR recombination is practically absent. On the other hand, after the SC has been fabricated, a p–n junction is formed near one of the wafer surfaces with significant recombination in the SCR at voltages up to the maximum power collection voltage $V = V_m$ with $V_m = 0.55{-}0.65\,\mathrm{V}$. This is explained by the fact that the SRH

lifetime in the SCR is always significantly lower than the SRH lifetime in the quasineutral region.[43,53,54] In turn, this is caused by the fact that the concentration of deep impurities is usually much higher in the SCR than in the quasineutral region.

A similar situation occurs when silicon is passivated with the dielectric layers of SiN_x or Al_2O_3, and a significant charge is built into the dielectric.[53,54] In the case of a SiN_x passivation layer, this charge is positive, and in the case of Al_2O_3, it is negative. Then, near the surface of p-Si in the first case and n-Si in the second case, the conductivity inversion condition occurs and the recombination in the SCR becomes significant. This was confirmed[43,53,54] primarily by the fact that the dependence of the effective lifetime on excess concentration observed a maximum and a decrease in τ_{eff} in the region of $\Delta n < 10^{15}$ cm^{-3}. The lifetimes in SCR were significantly lower than in the neutral bulk of the base and were on the order of microseconds.[43,53,54]

The SCR recombination velocity was calculated as

$$S_{SCR}(\Delta n) = \int_0^w dx\,(n_0+\Delta n)\left[(n_0+\Delta n)\,e^{y(x)} + n_i\,e^{E_t/kT} + b_r\left((p_0+\Delta n)\,e^{-y(x)} + n_i\,e^{-E_t/kT}\right)\right]^{-1}\tau_{SCR}^{-1}(x). \quad (19)$$

Here, $b_r = C_p/C_n = V_{pT}\sigma_p/(V_{nT}\sigma_n)$ is the ratio of the hole and electron capture coefficients, expressed as products of the respective thermal velocities $V_{(p,n)T}$ by the capture cross sections $\sigma_{p,n}$, $\tau_{SCR} = (V_{pT}\sigma_p N_t^*)^{-1}$ is the hole lifetime in the SCR, N_t^* is the concentration of deep impurities in the SCR, n_0 and p_0 are the equilibrium electron and hole concentrations, $y(x)$ is the electric potential divided by the thermal voltage kT/q, E_t is the energy of the deep impurity measured from the middle of the band gap, and w is the SCR width found from

$$w = \int_{y_0}^{y_w} dx\,\frac{L_D}{\sqrt{\left(1+\frac{\Delta n}{n_0}\right)(e^y-1) - y + \frac{\Delta n}{n_0}(e^{-y}-1)}}, \quad (20)$$

where y_0 is the non-dimensional potential at the boundary between the n- and p-regions, y_w is the non-dimensional potential at the boundary between the SCR and the quasineutral regions, and $L_D = \sqrt{\varepsilon_0\,\varepsilon_{Si}\,kT/(2q^2n_0)}$ is the Debye screening length. In the calculations, we took $y_w = -0.1$.

When $\tau_{SCR}(x) = \text{const.}$, the integral (19) can be simplified as follows. Changing the integration variable from the position x to the non-dimensional potential y, we have

$$S_{SCR}(\Delta n) = \int_{y_w}^{y_0} dy\,(n_0+\Delta n)\,F\left[(n_0+\Delta n)\,e^{y} + n_i\,e^{E_t/kT} + b_r\left((p_0+\Delta n)\,e^{-y} + n_i\,e^{-E_t/kT}\right)\right]^{-1}\tau_{SCR}^{-1}, \quad (21)$$

where

$$F = \frac{L_D}{\sqrt{\left(1+\frac{\Delta n}{n_0}\right)(e^y-1) + y_m + \frac{p_0+\Delta n}{n_0}(e^{-y}-1)}}. \quad (22)$$

In the following, we will analyze the case when the deep impurity level E_t is in the middle of the bandgap; then, the terms that multiply n_i in (21) can be neglected.

The non-dimensional potential $y(x)$ can be found from Poisson's equation, whose solution reads

$$x = L_D\int_{y_0}^{y}\frac{dy'}{\sqrt{\left(1+\frac{\Delta n}{n_0}\right)(e^{y'}-1) - y' + \frac{\Delta n}{n_0}(e^{-y'}-1)}}. \quad (23)$$

The non-dimensional potential y_0 at $x = 0$ is found from the neutrality equation

$$qN = \sqrt{2kT\,\varepsilon_0\varepsilon_{Si}} \times \sqrt{(n_0+\Delta n)(e^{y_0}-1) - n_0y_0 + \Delta n(e^{-y_0}-1)}, \quad (24)$$

where qN is the surface charge density of acceptors in the pn junction.[43]

When the voltage applied to the pn-junction increases, or when the SC is illuminated, the value of y_0 decreases, and so does the SCR width w. That is, part of the SCR becomes neutral. In the region that has become neutral, recombination also occurs, the rate of which is equal to

$$S_{SCR-n} = \frac{w(\Delta n=0) - w(\Delta n)}{\tau_{SCR}}\,\frac{n_0+\Delta n}{n_0+\Delta n + b_r\Delta n}. \quad (25)$$

For highly efficient silicon SCs, the value of S_{SCR-n} is of a similar order of magnitude as S_{SCR} at the points of maximum power and open circuit. This is because the lifetimes in the SCR are much shorter than the lifetimes in the neutral base. Therefore, when calculating the SCR recombination velocity, one should use the expression in which both components are taken into account

$$S_{SCR-tot} = S_{SCR} + S_{SCR-n}. \quad (26)$$

In further analysis, we will use this expression for the total recombination velocity in the SCR.

IV. EXPRESSIONS FOR CALCULATING THE SC CHARACTERISTICS

In this section, we summarize the expressions used to calculate the light and dark dependencies and the efficiency of photoconversion. The illuminated $I-V$ curve is calculated with the help of the

following expressions:

$$\begin{aligned} I_L(V) &= I_{SC} - I_r(V) + \tfrac{V+I_L R_S}{R_{SH}}, \\ I_r(V) &= qA_{SC}\left(\tfrac{d}{\tau_{eff}^b} + S_0\left(1+\tfrac{\Delta n}{n_0}\right) + S_{SC-tot}\right)\Delta n(V). \\ \tau_{eff}^b &= \left(\tfrac{1}{\tau_{SRH}} + \tfrac{1}{\tau_{exc}} + \tfrac{1}{\tau_r} + \tfrac{1}{\tau_{Auger}}\right)^{-1}, \\ \Delta n &= -\tfrac{n_0}{2} + \sqrt{\tfrac{n_0^2}{4} + n_i^2(T,\Delta E_g)(e^{q(V+I_L R_s)/kT}-1)^2}. \end{aligned} \tag{27}$$

Here, $I_L(V)$ is the net current, I_{SC} is the short-circuit current, $I_r(V)$ is the recombination (dark) current, A_{SC} is the SC surface area, R_s and R_{SH} are the series and shunt resistance, and ΔE_g is the band gap narrowing of Si. The lifetimes τ_{exc}, τ_r, and τ_{Auger} depend on the total concentration $n = n_0 + \Delta n$ of electrons in the base region according to Eqs. (8), (13), and (15), respectively.

These expressions allows to obtain the open-circuit voltage by setting $I_L = 0$ and $\Delta n(V_{OC}) = \Delta n_{OC}$,

$$V_{OC} = \frac{kT}{q}\ln\left(1 + \frac{\Delta n_{OC}(n_0+\Delta n_{OC})}{n_i^2(T)\,e^{\Delta E_g/kT}}\right). \tag{28}$$

Multiplying the current $I_L(V)$ by the applied voltage V, we obtain the power $P(V)$, and from the condition of maximum $dP/dV = 0$, we find the value of the voltage at the point of maximum power collection V_m. By substituting V_m into the first equation (27), we obtain the value of the current I_m at maximum power. This allows to calculate the efficiency η of photoconversion and the fill factor FF of the $I-V$ curve in the usual way

$$\eta = \frac{I_m V_m}{P_S}, \quad FF = \frac{I_m V_m}{I_{SC} V_{OC}}, \tag{29}$$

where P_S is the incident energy flux density under the AM1.5 conditions.

The dark current is given by

$$\begin{aligned} I_d(V) &= \tfrac{qA_{SC} d\,\Delta n}{\tau_{eff}(\Delta n)} - \tfrac{V - I_d R_s}{R_{SH}}, \\ \Delta n &= -\tfrac{n_0}{2} + \sqrt{\tfrac{n_0^2}{4} + n_i^2(T,\Delta E_g)(e^{q(V-I_d R_s)/kT}-1)}. \end{aligned} \tag{30}$$

Finally, the short-circuit current is related to the open-circuit voltage by

$$\begin{aligned} I_{SC}(V) &= \tfrac{qA_{SC} d\,\Delta n_{OC}}{\tau_{eff}(\Delta n_{OC})} - \tfrac{V_{OC}}{R_{SH}}, \\ \Delta n_{OC} &= -\tfrac{n_0}{2} + \sqrt{\tfrac{n_0^2}{4} + n_i^2(T,\Delta E_g)(e^{q(V_{OC})/kT}-1)}. \end{aligned} \tag{31}$$

The effective lifetime can be related to the excess concentration either the short-circuit current vs the open-circuit voltage or using the dark current. Namely,

$$\tau_{eff} = qd\,\frac{\Delta n_{OC}}{J_{SC}} = qd\,\frac{\Delta n(V)}{J_d(V)}. \tag{32}$$

When I_{SC} vs V_{OC} is measured, the excess carrier density $\Delta n_{OC} = \Delta n(n_0, V_{OC})$, and the procedure of finding $\tau_{eff}(\Delta n)$ is quite straightforward. On the other hand, when one uses the dark $I--V$ curve, the excess concentration depends on many parameters, namely, $\Delta n = \Delta n(n_0, R_s, V, I_L)$.

V. COMPARISON OF THE EXPERIMENTAL RESULTS WITH THE THEORY

A. Photoelectric characteristics

We apply the formalism above to (i) the Sanyo HIT SC,[55,56] (ii) to a commercial SC with a p–n junction manufactured by the SunPower technology (see Ref. 57 for details), (iii) the Silicon Hetero Junction (SHJ) SC from Ref. 58, and (iv) to the SHJ SC with the record for efficiency to date from Ref. 18.

In Fig. 3, the experimental $EQE(\lambda)$ curves measured (a) by Yoshikawa *et al.*[58] and (b) by Lin *et al.*,[18] are compared with the calculated ones. The experimental curves were fitted with Eq. (2) in the long-wavelength ($\lambda > 800$ nm) part of the spectrum by varying the parameter b, which turned out to have the value of 1.8 and 1.6, respectively. Once the parameter b is established, expressions (1) and (2) are used to predict how the short-circuit current depends on the base thickness d.

Let us consider the inaccuracy that can arise from neglecting recombination in the SCR or trap-assisted Auger exciton recombination in the SC simulation. This analysis is performed for the SCs mentioned above based on the respective experimental results and the theory developed in this work.

The results are summarized in Table I, which presents the experimental data for the photoconversion efficiency η_{exp} and the effective lifetimes τ_{exp} at the maxima of the $\tau(\Delta n)$ curves found in the literature.[18,55–58] Also indicated in this table are the theoretical photoconversion efficiency η^0_{theory1} found under the assumption

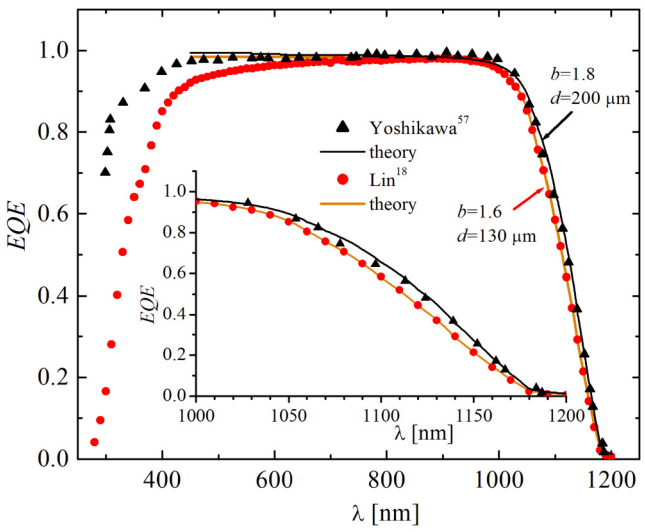

FIG. 3. Symbols: experimental dependence of the external quantum efficiency $EQE(\lambda)$, as measured by Yoshikawa *et al.*[58] (triangles) and Lin *et al.*[18] (circles). The theoretical fit (solid lines) of the long-wavelength ($\lambda > 800$ nm) part of the graph with Eq. (2) yields the parameter $b = 1.8$ i and $b = 1.6$ accordingly.

TABLE I. Experimental photoconversion efficiencies and maximum lifetimes for the SCs are taken from the articles listed in the first column. Theoretical efficiencies are obtained without accounting for SCR or trap-assisted exciton Auger recombination, and the lifetimes are calculated by assuming that the SCR recombination lifetime is the same as the SRH lifetime in the bulk. The parameters $\Delta_{\eta_{1,2}}$ represent the loss due to recombination in the SCR and trap-assisted exciton Auger recombination, while Δ_τ represents the ratio of the theoretical to the experimental maximum lifetime, respectively.

SC (Reference)	η_{exp}, %	$\eta^0_{theory1}$, %	Δ_{η_1}, %	$\eta^0_{theory2}$, %	Δ_{η_2}, %	τ_{exp}, ms	τ_{theory}, ms	Δ_τ
Taguchi *et al.*[55,56]	21.5	22.15	3.0	21.62	0.56	0.58	1.13	1.95
Sachenko *et al.*[57]	21.8	22.18	1.74	21.83	0.14	2.82	8.83	3.13
Yoshikawa *et al.*[58] and Sachenko *et al.*[59]	26.63	26.91	1.05	26.87	0.9	7.08	13.27	1.87
Lin *et al.*[18]	26.81	27.26	1.7	26.89	0.3	5.15	18.7	3.63

that the SCR recombination is absent, $\eta^0_{theory2}$ is the theoretical efficiency of photoconversion when Auger exciton recombination is neglected, and the maximum lifetimes are calculated with the assumption that the SCR lifetime equals the SRH lifetime in the base region. The parameters $\Delta_{\eta_1} = [(\eta^0_{theory1}/\eta_{exp}) - 1] \times 100\%$ is the loss due to recombination in the SCR, and $\Delta_{\eta_2} = [(\eta^0_{theory2}/\eta_{exp}) - 1] \times 100\%$ is the loss due to trap-assisted exciton Auger recombination, respectively.

As can be seen in Table I, the efficiency losses in the considered SCs due to recombination in the SCR range between 1% and 3%, while the losses due to Auger exciton recombination via traps are up to 1%. At the same time, the effective lifetimes of these SCs, when recombination in the SCR is neglected (i.e., when the lifetime in the SCR is assumed to be equal to the SRH lifetime in the base region), increase by more than 100%. This is because at the point of the maximum effective lifetime, recombination in the SCR is greater than the sum of the contributions from recombination through all other channels, including surface recombination. As for the photoconversion efficiency, the point of maximum power output for high-efficiency silicon solar cells lies to the right of the maximum effective lifetime, where the recombination rate in the SCR is lower. Therefore, the impact of recombination in the SCR on photoconversion efficiency is smaller. As shown in our previous work,[43] the losses related to recombination in the SCR are the greater the shorter the lifetime in the SCR. For example, our estimates of recombination losses in the SCR for the solar cells from the study,[56] assuming a recombination lifetime in the SCR of 10^{-6} s and $b_r = 1$ (see Ref. 53), are 7.3%.

In the work of Spinelli *et al.*,[60] the effect of recombination in the SCR on the photoconversion efficiency of the silicon SC studied by the authors is discussed. While the paper does not provide a detailed theory, the observed increase in efficiency in the absence of SCR recombination correlates with the values given in Table I.

The experimental total recombination velocity in the SCR and in that part of the SCR that has become neutral is found from

$$S^{exp}_{SCR-tot} = d\left(\left(\tau^{exp}_{eff}\right)^{-1} - \tau^{-1}_{SRH} - \tau^{-1}_{ex} - \tau^{-1}_{S} - \tau^{-1}_{Auger} - \tau^{-1}_{r}\right). \quad (33)$$

The theoretical SCR recombination velocity is found from expression (26). Figure 4 shows the experimental and theoretical dependencies of the recombination rate in the SCR on the excess concentration, obtained using the parameters from Yoshikawa *et al.*[58] As can be seen from the figure, the theoretical and experimental dependencies agree well with each other. The figure also shows that at an excess concentration of the order of 3×10^{15} cm^{-3}, which corresponds to the excess concentration at the point of maximum power, the two contributions to expression (26), namely, the SCR recombination velocity S_{SCR} and the recombination velocity in the region that has become neutral, S_{SCR-n}, become comparable.

Figure 5 shows the theoretical SCR recombination velocity $S_{SCR-tot}(\Delta n)$ curves for all the SCs that appear in Table I, both the p–n junction-based ones and the SHJ SC. In addition, Fig. 5 shows $S_{SCR-tot}(\Delta n)$ curve for the SC described in Ref. 32, with the respective calculation performed in Ref. 44 (red dashed-dotted curve). It turned out to have the smallest value of all the SCs analyzed here.

Three curves in Fig. 5 are plotted for SHJ elements, and two are for p–n junction SCs. The poorer the surface passivation, the shorter the SCR lifetimes (see the two upper curves); the SCR recombination velocity decreases with the surface passivation quality (three further curves). At first glance, the shorter SCR

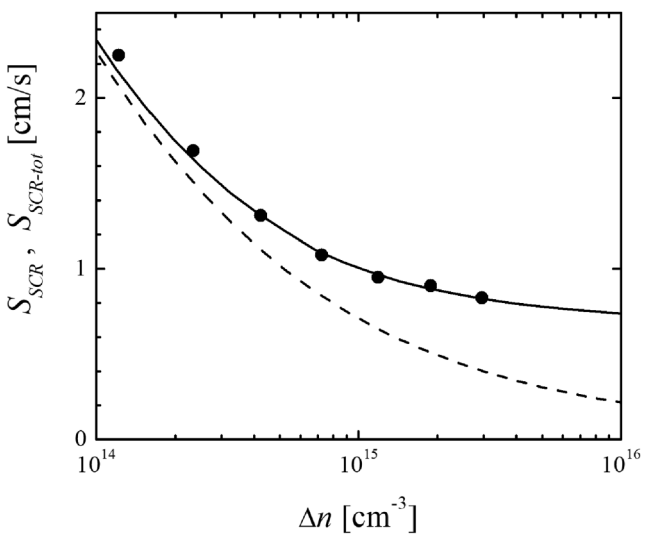

FIG. 4. The SCR recombination velocity S_{SCR} (dashed line) and the total SCR recombination velocity $S_{SCR-tot}$ (solid line) vs the excess concentration Δn (black circles), obtained for the SC of Yoshikawa *et al.*[58] Dashed line: theoretical curve (2). Solid line: the total surface recombination velocity (26).

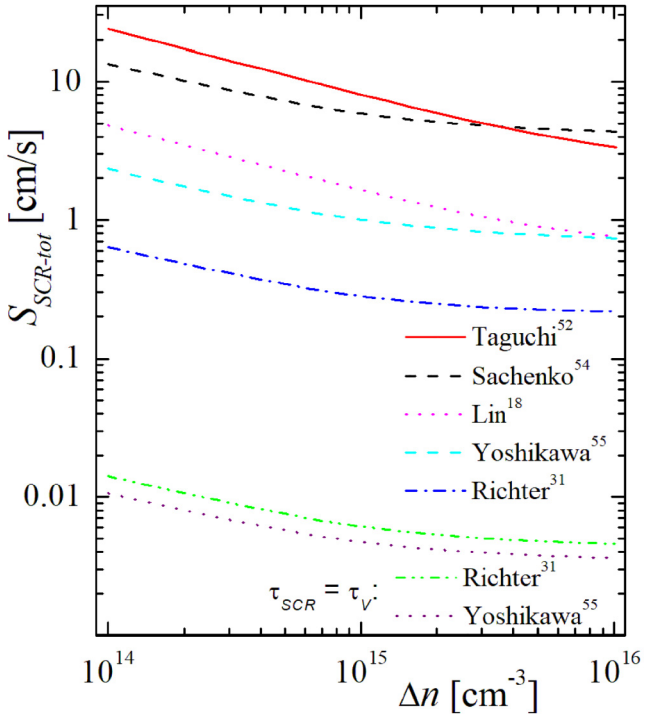

FIG. 5. Theoretical total SCR recombination velocity $S_{SCR-tot}$ vs the excess concentration Δn, plotted using the experimental data (from top to bottom) of Taguchi *et al.*,[55] Sachenko *et al.*,[57] Lin *et al.*,[18] Yoshikawa *et al.*,[58] and Richter *et al.*[32] The two lowest theoretical curves are plotted under the assumption that the lifetime in the SCR is equal to the bulk lifetime in the sample discussed in Richter *et al.*[32] (top) and Yoshikawa *et al.*[58] (bottom).

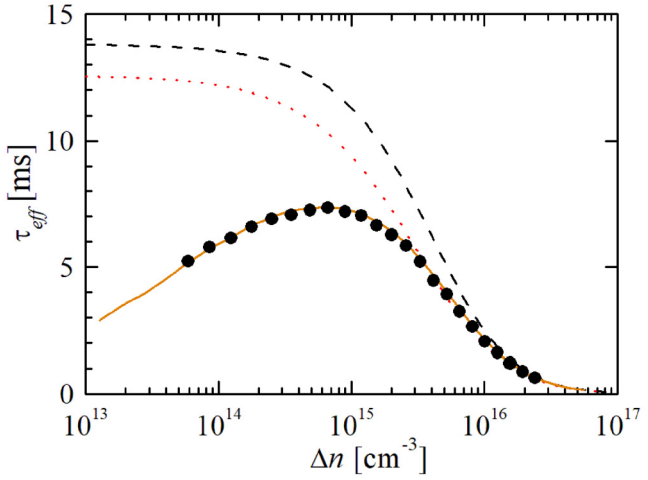

FIG. 6. Effective lifetime vs excess concentration in an SC from the work of Yoshikawa *et al.*[58] Symbols: experimental data. Solid line: theoretical curve. Dashed: The theoretical curve is plotted assuming that the SCR recombination time equals the bulk value. Dotted line: a theoretical curve with SCR recombination neglected and the surface recombination velocity set to 0.16 cm/s.

lifetimes should be found in the p–n junction SCs: the high-temperature operations are used in their manufacturing, accompanied by the impurity gettering in the SCR. However, this is not observed. If the SCR lifetimes had not decreased compared to the SRH lifetimes, then the SCR recombination velocities would have been ≤ 0.01 cm/s (see the two lower curves). In this case, the SCR recombination would practically not affect either the efficiency or the effective lifetimes of the excess charge carriers.

The theoretical effective lifetimes vs the excess concentration of charge carriers are calculated both for the SCR lifetime equal to $\tau_{SCR} = 79\,\mu$s determined for this SC (solid curve in Fig. 6) and also under the assumption that the SCR lifetime is the same as the SRH lifetime in the quasineutral base region, $\tau_{SRH} = 15.5$ ms (dashed line in Fig. 6). It can be seen from the figure that both the position and the height of the maximum of the experimental curve are correctly reproduced for $\tau_{SCR} = 79\,\mu$s. The value at the maximum effective lifetime obtained assuming $\tau_{SCR} = \tau_{SRH} = 15.5$ ms significantly (almost twice) exceeds the maximum value of the effective lifetime in the SCR in this SC.

At first glance, such a decrease in the lifetime amplitude can be attributed to surface recombination. However, the calculations show that if the SCR recombination is neglected, then it is possible to achieve agreement between the theoretical and the experimental effective lifetime only at relatively high excess carrier concentration $\Delta n > 3 \times 10^{15}$ cm^{-3} (see the dotted curve in Fig. 6). A similar situation is observed for other SCs analyzed. Thus, if the efficiency of the investigated SCs increases by neglecting the SCR recombination by only about 1%, the situation is completely different for the effective lifetimes. Not to mention the fact that the region falling towards small excess concentrations exists for all SCs and, with very few exceptions, is explained by recombination in the near-surface region of the SC base. Thanks to the SCR recombination, the effective lifetime near the maximum significantly decreases, a fact to which little attention was paid until recently.

Thus, as the above analysis shows, the SCR recombination not only ensures the decrease of the effective lifetime in the SCs studied at sufficiently small excess concentrations but also strongly affects its maximum value. Moreover, even in the case of a high surface recombination velocity[55] $S_0 = 8.2$ cm/s, the effect of recombination in the SCR on the photoconversion efficiency exceeds the impact of surface recombination. In this case, the actual photoconversion efficiency of 21.5% increases to 21.9% if surface recombination is neglected and to 22% if recombination in the SCR is also neglected.

In the SCs with well-passivated surfaces, surface recombination affects the efficiency much less than the recombination in the SCR. For example, for the SCs reported by Yoshikawa *et al.*,[58] neglecting the SCR recombination leads to an increase in efficiency by 1%, while neglecting surface recombination increases the efficiency by 0.12%. Since the SCR recombination has a stronger effect than the surface recombination, which is always taken into account, the SCR recombination must also be considered in SC modeling.

Let us now analyze the SC output power dependence on the applied voltage. Figure 7 shows this curve for the SCs from Ref. 55 (symbols), compared to the theoretical curves obtained in the approximations of six and four recombination channels. Within

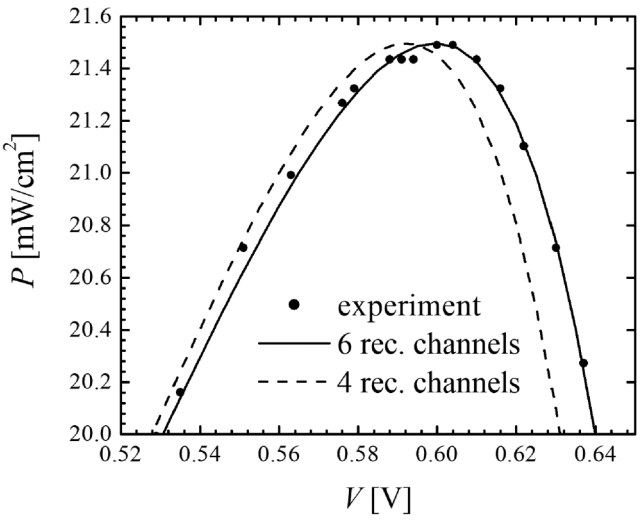

FIG. 7. Output power P vs voltage V across the solar cell, measured experimentally in Taguchi *et al.*[55] (symbols), and calculated theoretically under the approximation of six and four recombination channels operative in the SC (solid and dashed lines, respectively). In the four-channel approximation, SRH, radiative, Auger, and surface recombination mechanisms are taken into account. The non-radiative exciton Auger recombination and the SCR recombination in the six-channel calculation are also included.

the four-channel model, SRH, radiative, Auger, and surface recombination processes are taken into account. The non-radiative exciton Auger recombination and the SCR recombination in the six-channel calculation are also included. It can be seen that near the point of maximum power $V_m = 599\,\text{mV}$, the six-channel approximation agrees with the experiment. Although at $V < V_m$, the curves built in these approximations differ only slightly, the discrepancy between them is much greater at $V > V_m$. The locations of the maxima predicted by the two models differ by 7 mV, which exceeds the error of voltage measurements.

B. Choice of the approximation for Auger recombination rate

Several approximate formulas exist for the band-to-band Auger recombination rate as a function of the excess charge carrier concentration.[13,14,30,52]

However, except for a few papers,[18] we are not aware of a comprehensive discussion of the approximation choice for calculating the photoconversion efficiency of highly efficient silicon SCs. Although the effective lifetime changes insignificantly when using different approximations, for sufficiently large excess carrier concentrations, specifically when $\Delta n \geq 10^{16}\,\text{cm}^{-3}$, the obtained $\tau(\Delta n)$ curves deviate somewhat more substantially from one another.

A different situation occurs when fitting the illuminated $I-V$ curves and the output power dependence on the applied voltage. While analyzing the experimental illuminated $I-V$ characteristics of the solar cell,[18] we found that the values of the open circuit voltage observed in this work cannot be reproduced theoretically using the approximations of Richter *et al.*,[52] Black *et al.*,[30] and Niewelt *et al.*[13] When analyzing the SCs whose surfaces are passivated so well that the surface recombination velocity becomes smaller than 1 cm/s, it becomes important which approximation to use. In the opposite case of surface recombination velocities exceeding 1 cm/s, all approximations for Auger recombination time work equally well.

This observation is illustrated by Fig. 8(a) showing the inverse Auger recombination time $1/\tau_{Auger}$ obtained within

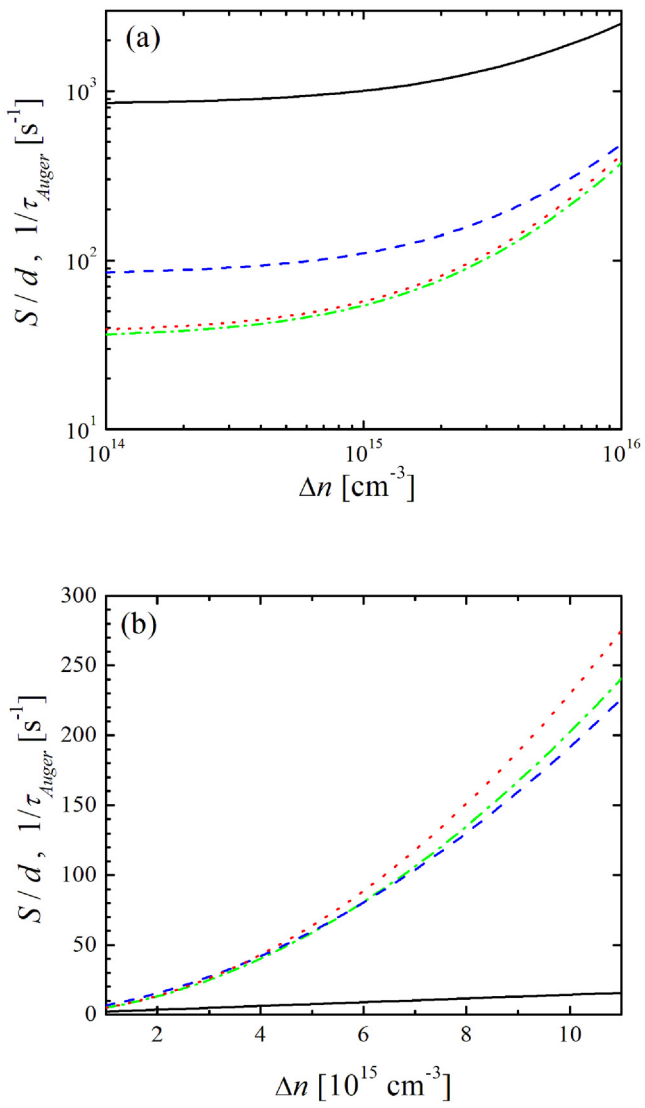

FIG. 8. Solid black curves: surface recombination velocity divided by the base thickness from (a) Ref. 55 (doping level $n_0 = 5 \times 10^{15}\,\text{cm}^{-3}$) and (b) Ref. 18 (doping level $n_0 = 6.5 \times 10^{14}\,\text{cm}^{-3}$). Colored curves: inverse Auger lifetime in various approximations, namely, Richter *et al.*[10] (blue dashed line), Niewelt *et al.*[13] (red dotted line), and Veith-Wolf *et al.*[14] (green dashed-dotted line).

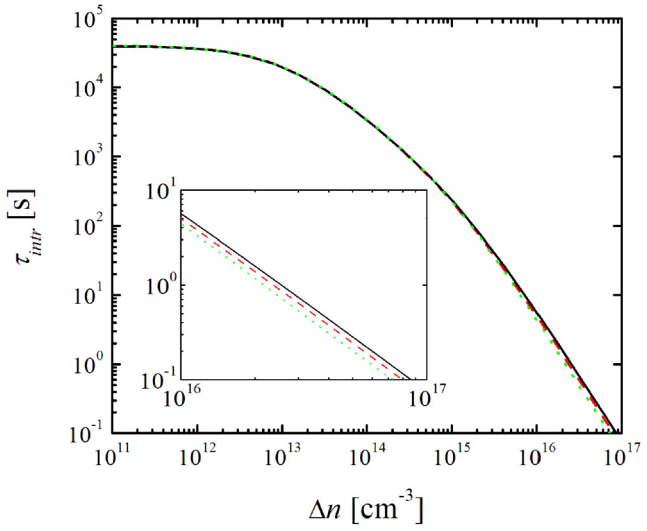

FIG. 9. Intrinsic effective (radiative and Auger) lifetime in Si vs the excess carrier concentration. The inset shows the same plot at Δn above 10^{16} cm^{-3}.

different approximations vs the excess concentration Δn for the SC described in Ref. 55. In this figure, the black solid line shows the surface recombination velocity divided by the base thickness S/d, that is, the inverse of the surface recombination time, which significantly exceeds the inverse Auger lifetimes. Therefore, the surface recombination velocity can be found to a good accuracy no matter which approximation is used for the Auger lifetime.

However, the choice of the approximation matters when the surface recombination velocity is significantly lower than 1 cm/s. This is the case in the record-efficiency SCs from Ref. 18, see Fig. 8(b), in which $S = 0.017$ cm/s, with the respective inverse lifetime S/d significantly smaller than the inverse lifetimes of Auger recombination in all three approximations. As can be seen from Fig. 8(b), the formula from Veith-Wolf *et al.*[14] gives a smaller inverse time than the approximation used by Niewelt *et al.*[13] The latter expression allows us to calculate the open circuit voltage in the SC from Ref. 18 to be about 747 mV, whereas its experimental value equals 751.4 mV.

Let us further consider the intrinsic recombination limit using for the calculations the parameters from Ref. 12, namely, $J_{SC} = 0.0434$ A/cm^2, $d = 63.3\,\mu$m, and $n_0 = 10^{13}$ cm^{-3}. Figure 9 shows in the double-logarithmic scale the dependence of the effective intrinsic lifetime $\tau_{intr}^{-1} = \tau_{rad}^{-1} + \tau_{Auger}^{-1}$ in silicon on the excess carrier concentration for the three Auger recombination time approximations, proposed by Richter *et al.*,[52] Veith-Wolf *et al.*,[14] and Nievelt *et al.*,[13] respectively.

As can be seen from the figure, in the region $\Delta n < 10^{15}$ cm^{-3}, the curves in the double-logarithmic scale practically coincide. The difference is more pronounced in the semi-logarithmic scale (not shown here). At $\Delta n > 10^{15}$ cm^{-3}, the effective lifetime curves calculated using different approximations deviate from each other more substantially (see the inset in Fig. 9). The effective lifetime curve, plotted using the approximation of Richter *et al.*[52] is most strongly shifted to the right toward higher concentrations. The $\tau_{eff}(\Delta n)$ curve obtained from the formula of Veith-Wolf *et al.*[14] is shifted to the left towards lower concentrations, while the curve constructed using the approximation of Niewelt *et al.*[13] goes even further to the left. In general, as can be seen from Fig. 9, the dependencies of the effective lifetime on the excess concentration differ slightly for different approximations for the Auger recombination. Even when $\Delta n = 10^{17}$ cm^{-3}, the largest difference between them is 33%, which is not much in these conditions.

To choose the approximation for the Auger recombination rate when modeling the performance of well-passivated SCs, as investigated in Refs. 18 and 58, it is useful to analyze their key parameters in the intrinsic recombination limit. As our calculations demonstrate, for the SCs from Ref. 58, the excess concentration in the open-circuit mode is about 1.6×10^{16} cm^{-3}, and for the SCs from Ref. 18, it is about 2×10^{16} cm^{-3}. Table II shows the key parameters for the SCs with doping levels of 6.5×10^{14} cm^{-3}, which corresponds to the case of Ref. 58, and 3.23×10^{15} cm^{-3}, which was implemented in Ref. 18, in the intrinsic recombination limit using three approximations for the Auger recombination rate from Refs. 13, 14, and 52. We did not consider the approximation from Ref. 30 separately because we believe that when obtaining the approximation from Ref. 13, the results presented in Ref. 30 were taken into account.

Table II shows the values of the open-circuit voltage V_{OC}, excess concentrations in the open-circuit regime Δn_{OC}, and photoconversion efficiency η obtained for three approximations for Auger recombination rate at two doping levels, which correspond to the ones used in Refs. 18 and 58. As can be seen from the table,

TABLE II. Open-circuit voltage V_{OC}, excess carrier concentration in the open-circuit mode Δn_{OC}, and photoconversion efficiency η_{intr} in the intrinsic recombination limit in the SC of thickness $d = 63.3\,\mu$m and doping level $n_0 = 6.5 \times 10^{14}$ cm^{-3} with three different approximations for the Auger recombination rate from the literature.

SC (Reference)	Doping level, cm^{-3}	V_{OC}, mV	Δn_{OC}, cm^{-3}	η_{intr}, %	Auger approximation
Yoshikawa *et al.*[58]	6.5×10^{14}	769.5	2.99×10^{16}	29.7	Richter *et al.*[52]
		767.5	2.88×10^{16}	29.69	Veith-Wolf *et al.*[14]
		764.6	2.70×10^{16}	29.6	Niewelt *et al.*[13]
Lin *et al.*[18]	3.23×10^{15}	766.9	2.72×10^{16}	29.1	Richter *et al.*[52]
		767.0	2.72×10^{16}	29.2	Veith-Wolf *et al.*[14]
		764.4	2.56×10^{16}	29.1	Niewelt *et al.*[13]

the experimental values of Δn_{OC} are close to those obtained in the intrinsic recombination limit. Therefore, if a particular approximation gives the highest open-circuit voltage and photoconversion efficiency, then it should also apply for the passivated SCs with the surface recombination velocity $S_0 \ll 1$ cm/s. In addition, the expressions for the photoconversion efficiency in the intrinsic recombination limit do not include such important parameters as series resistance. In actual SCs, the series resistance is always present and can significantly affect the photoconversion efficiency. Therefore, a working approximation should be chosen when the series resistance can be ignored, which is one of the defining features of the intrinsic recombination limit.

Table II shows that when the doping level is $6.5\times\ 10^{14}$ cm^{-3}, the highest open-circuit voltage and photoconversion efficiency are reached within the approximation proposed by Richter *et al.*,[32] and the smallest efficiencies are for the approximation of Niewelt *et al.*[13]

In contrast, for the doping level of 3.23×10^{15} cm^{-3}, the results obtained for the approximations of Richter *et al.*[32] and Veith-Wolf *et al.*[14] get interchanged, namely, the use of the approximation of Veith-Wolf *et al.* leads to the highest open-circuit voltage and photoconversion efficiency. As for the SC from Ref. 58, the best results are obtained with the approximation of Richter *et al.*,[32] which should be used when modeling its parameters. As for the SCs with substantial surface recombination, any approximation for the Auger recombination time can be used.

The key characteristics of the SCs we considered, namely, doping level N_d, base thickness d, open circuit voltage V_{OC}, short circuit current density J_{SC}, efficiency η, fill factor FF, and shunt resistance R_S are listed in Table III. The first four rows of Table III match those of Table I, while the last fifth row shows the key parameters of an optimized SC calculated within the formalism that we developed. It should be noted that all the calculated parameter values coincide with the experimental ones up to the third significant figure. Only in the fourth significant figure did the calculated $I-V$ curve fill factors slightly differ from the experimental values.

The sixth row of Table III shows the results of optimizing the parameters of the silicon SC obtained in the work of Khokhar *et al.*[37] using Quokka 3, that is, for the three-dimensional case. Unfortunately, the work[37] does not include the $EQE(\lambda)$ dependence, so we are unable to calculate the parameters presented there for comparison using the one-dimensional approximation we proposed. However, we can calculate the parameters for the optimized case (row 5 of Table III) in the one-dimensional approximation, assuming no recombination in the SCR and no trap-assisted exciton Auger recombination. The results of this calculation are presented in row 7 of Table III.

To achieve a photoconversion efficiency of 26.64% with the same optimal values for doping level (5×10^{15} cm^{-3}), base thickness (200 μm), when the Shockley–Read–Hall lifetime is 10 ms and the series resistance is 0.05 Ω cm^2 (sixth row, Khokhar *et al.*[37]), the parameters in the one-dimensional approximation should be as follows: initial surface recombination velocity S_0 = 1.47 cm/s and parameter $b = 2.36$. From a comparison of the SC parameters given in rows 5 and 7 of Table III, it can be seen that although the key SC parameters, when taking into account or not taking into account recombination in the SCR and non-radiative trap-assisted exciton Auger recombination, are similar, the difference in photoconversion efficiencies is 1.4%, while the smallest difference in optimal base thicknesses is 26%, and the difference in optimal doping levels is even greater. Thus, the results shown in Table III indicate that for accurate determination of the optimal doping levels and base thicknesses, recombination in the SCR and trap-assisted exciton Auger recombination must be considered.

C. Solar cell optimization

The theoretical expressions for the efficiency as a function of the doping level and the base thickness can be used to optimize the SCs with respect to these parameters. Figure 10 shows the photoconversion efficiency vs the doping level for the SC investigated by Yoshikawa *et al.*[58] As can be seen from this curve, the maximum efficiency is reached at the doping level close to 7×10^{15} cm^{-3}.

Figure 11 shows the dependence of the same SC's efficiency on the base thickness. It is seen that the highest efficiency is reached at the base thickness of 150 μm. These results and other parameters are given in the last row of Table III.

The closeness of the parameters obtained for the optimized sample from Ref. 58 and for the SC from Lin *et al.*[18] (fourth row of Table III) is striking. Note, in particular, changing the doping level in the optimized sample results in an increase of the open circuit voltage to 745.2 mV, making it almost equal to the one of the sample from Ref. 18. The calculated efficiency of the optimized SC, however, is higher than the efficiency of the record sample,[18] as can be seen from the last two rows of Table III.

Shown in Fig. 12 is the power vs voltage curve of an optimized sample using six and four recombination channels. In this case, the difference between the theoretical $I-V$ curves is visually almost imperceptible. To summarize this part, we can say that the theory

TABLE III. The key SC parameters published in the literature and those from Yoshikawa *et al.*,[58] but optimized for thickness and doping level to maximize efficiency, in the approximation of six (Optimized) and four (Optimized*) recombination channels.

SC (Reference)	n_0, cm^{-3}	d, μm	V_{OC}, mV	J_{SC}, mA/cm^2	η, %	FF, %	R_S, Ω cm^2
Taguchi *et al.*[56]	5×10^{15}	98	712.4	38.6	21.5	78.23	0.69
Sachenko *et al.*[45]	9×10^{14}	165	694	40.04	21.18	77.76	1.01
Yoshikawa *et al.*[58]	6.5×10^{14}	200	740.3	42.5	26.63	84.64	0.195
Lin *et al.*[18]	3.23×10^{15}	130	751.4	41.45	26.81	86.07	0.125
Optimized	7×10^{15}	155	744.8	41.8	27.01	86.80	0.195
Khokhar *et al.*[37]	5×10^{15}	200	737.9	42.06	26.64	85.85	0.05
Optimized*	4.5×10^{15}	195	739.5	42.2	26.7	85.5	0.297

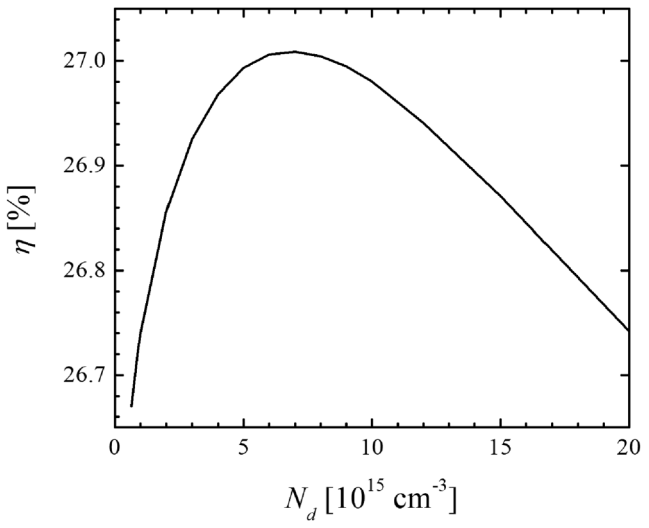

FIG. 10. Theoretical photoconversion efficiency vs the doping level for the SC investigated by Yoshikawa *et al.*[58] vs the doping level.

developed here allows for the finding of a number of optimal parameters from a simple calculation, whereas experimentally, the same optimization task would require a number of rather expensive operations.

D. Further improvement of the efficiency of silicon SCs

Recently, an updated table of high-efficiency SCs been published,[20] announcing that a new record of 27.3% has been set by the researchers from LONGi company. The article[20] also contains

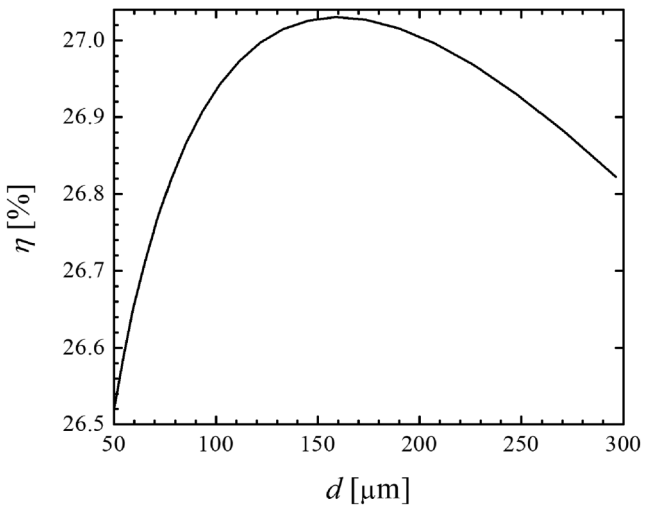

FIG. 11. Theoretical photoconversion efficiency vs the base thickness of the SC fabricated by Yoshikawa *et al.*[58]

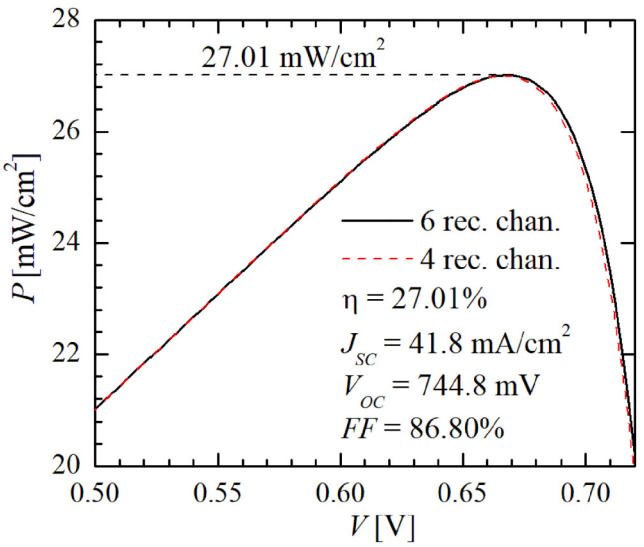

FIG. 12. The power vs voltage curve of an optimized SC from Ref. 58 with the recombination rate calculated using six (solid black line) and four (dashed red line) recombination channels.

the external quantum efficiency and the illuminated $J - V$ curve of this SC. Using the above theory, we calculated the power of this SC on the applied voltage and compared the results with the experiment. The obtained results are shown in Fig. 13. As can be seen from the figure, the agreement between the theory and the experiment is good.

The results of this analysis are also found in Table IV, which summarizes the parameters of both LONGi SCs.[18,20]

In addition, we calculated the efficiency of two hypothetical SCs, in which the SRH lifetime was increased, and it was also assumed that the lifetime in the SCR was equal to the Shockley–Reed–Hall lifetime. These are the third and fourth entries in the Table IV. In the case of the third element, the lifetime is τ_{SRH} was set equal to 50 ms, and for the fourth one to 100 ms. Samples of n-Si with the lifetime of 111 ms (with $n_0 = 9.43 \times 10^{13}$ cm^{-3}) and above 200 ms (with $n_0 = 6.5 \times 10^{12}$ cm^{-3}) were investigated in Refs. 13 and 30. A strong efficiency increase in these SCs is associated with a decrease in the recombination rate in the SCR. If their lifetime remained equal to 5×10^{-2} ms, then the efficiency of the third SC would be 27.56 %, and the fourth would be 27.77%. As can be seen, the reduction of the efficiency is significant. This once again emphasizes the need to obtain longer lifetimes for recombination in the SCR.

VI. PRACTICALLY ACHIEVABLE MAXIMUM EFFICIENCY OF CRYSTALLINE SILICON SOLAR CELLS

Various approaches can be used to assess the practically achievable highest efficiency of the crystalline silicon SCs.

We propose to combine the parameters of the best-performance SCs to date. Thus, the maximum practically attainable

TABLE IV. Parameters of the SC produced by the LONGi company[18] with the efficiency of 26.81%, the recently reported[20] SC with the record efficiency of 27.3%, and two hypothetical SCs with long SRH lifetimes in the base and the SCR.

SC	J_{SC}, mA/cm^2	V_{OC}, mV	FF, %	η, %	n_0, 10^{15} cm^{-3}	d, μm	τ_{SRH}, ms	τ_{SCR}, ms	R_S, Ω cm^2	R_{sh}, Ω cm^2
Lin *et al.*[18]	41.45	751.4	86.1	26.81	3.23	130	35	0.05	0.125	10^4
Lin *et al.*[20]	42.6	743.4	86.2	27.3	3.23	200	35	0.05	0.15	10^5
Hypothetical 1	42.6	744.4	86.9	27.56	3.23	200	50	50	0.15	10^5
Hypothetical 2	42.6	745.2	87.5	27.77	3.23	200	100	100	0.15	10^5

short-circuit current is the one with the smallest coefficient b in Eq. (12), which describes the deviation of absorptance from the Lambertian limit. The smallest value $b = 1.6$ is obtained by fitting the short circuit current of the record-efficiency SCs.[18] Next, the lowest optical losses due to reflection and absorption outside of the SC make up 1%, as can be deduced by fitting experimental data.[58] These parameters give us the short-circuit current density of 43.09 mA/cm^2.

We set the surface recombination velocity to 0.01 cm/s and the series resistance[18] to 0.125 Ω cm^2. Furthermore, we take the thickness of the base region to be 110 μm, the shunt resistance[58] of 300 kΩ cm^2,[58] the SRH lifetime both in the base region and in the SCR is taken to be 0.05 s, the doping level of 5×10^{15} cm^{-3}.

The dependence of the power on the applied voltage of the SC constructed in this way is shown in Fig. 14. The efficiency calculated from them is 27.79%. This value exactly coincides with the achievable efficiency calculated earlier[61] for a one-sided SC.

Thus, it follows from the results of our analysis that the practically achievable efficiency of heterojunction SCs is around 27.79%. It can be concluded that the LONGi SC with a photoconversion efficiency of 27.3%[20] is very close to the practical limit in terms of photoconversion efficiency as it is characterized by minimal values of surface recombination velocity and recombination rates in the SCR due to very effective passivation, as well as the best light trapping coefficient $b = 1.6$ compared to other SCs.

Therefore, after reaching the practical limit of photoconversion efficiency, we see further prospects for heterojunction silicon SCs in their use as a bottom part in tandem with wide-bandgap perovskite semiconductors, despite their somewhat overestimated bandgap compared to the optimal for tandems; this, however, does not lead to a significant decrease in the total efficiency. Organic–inorganic perovskite films, like heterojunction silicon SCs, are characterized by low-temperature manufacturing technology, which is important, and their record efficiency for an area of about 1 cm^2 reached 25.2%.[20] Research in the direction of creating perovskite/silicon tandem SCs gives very encouraging results, in particular, monolithic two-contact tandem perovskite/silicon SCs have been reported with the record efficiency values,[20,62] which are 34.2% for an area of 1 cm^2 and 28.6% for an area of 258.14 cm^2.

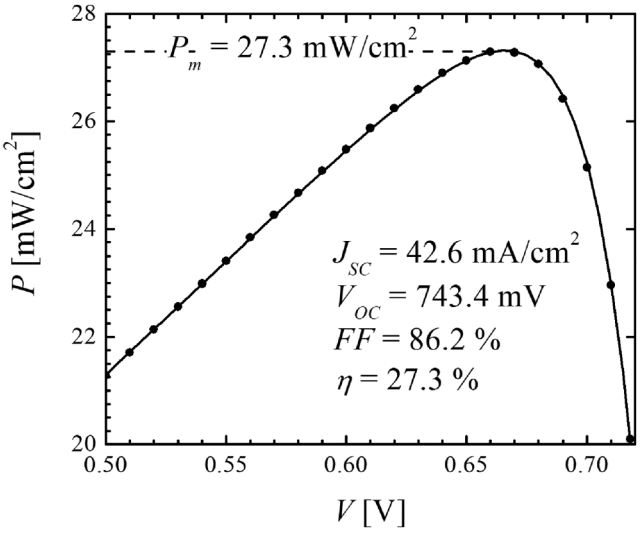

FIG. 13. Output power vs applied voltage for a SC with the record efficiency of 27.3%.[20] Symbols: experiment; solid line: theory.

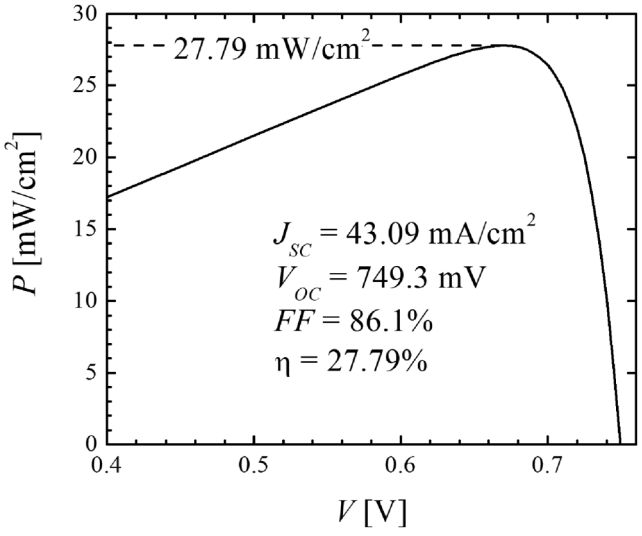

FIG. 14. Output power vs voltage of a hypothetical SC with the practically achievable photoconversion efficiency.

VII. CHALLENGES TO BE ADDRESSED TO REDUCE THE SCR RECOMBINATION

Contrary to the common point of view that the main source of losses in high-efficiency c-Si is surface recombination, the analysis carried out in this work shows that this is not the case. Greater losses are caused by recombination in the SCR, which inevitably exists in every silicon SC, because in each element there is a conductivity inversion, at which the recombination in the SCR is maximal. An additional problem is that in practical SCs, the SCR lifetime is significantly shorter than in the quasineutral base region.

This applies not only to SCs. A similar situation occurs when silicon is passivated by SiN_x or Al_2O_3 layers,[53,54] when a significant charge is built into the dielectric, as discussed earlier in Sec. III. The SCR lifetimes must be significantly shorter than in the neutral bulk of the base and are of the order of $0.1-1\,\mu s$.[53,54]

From the results presented in this work, it follows that surface passivation, which reduces the surface recombination velocity, also leads to a decrease in the SCR recombination rate. However, there are not enough statistics here to state this for sure. In our opinion, it is worth carrying out targeted research devoted to the analysis of the regularities of the recombination in the SCR and the development of ways to reduce it.

VIII. CONCLUSIONS

In this paper, we first briefly review the progress in the research field of monocrystalline silicon-based photovoltaics. Second, we discuss the semi-analytical formalism, developed to comprehensively characterize and optimize the highly efficient SCs based on monocrystalline silicon. Third, using the formalism developed, we performed analysis and optimized the record-breaking c-Si SCs.

A numerical parameter is introduced with an analytical expression, which allows for obtaining accurate reproduction of the theoretical wavelength-dependent external quantum efficiency EQE in the long-wavelength absorption spectral region. The theoretical $EQE(\lambda)$ curves that were obtained are consistent with the experimental ones.

It has been established that the full characterization of these SCs cannot be carried out without measurements and appropriate processing of the dark $I-V$ characteristics or, alternatively, of the short-circuit current on open-circuit voltage. We proved that it is not possible to reconcile the dependence of the output power on the applied voltage $P(V)$ and the effective lifetime of non-equilibrium charge carriers on the excess concentration with the experiment, without taking into account the recombination in the space charge region (SCR). It should be emphasized that taking recombination in the SCR into account is important when constructing a two- or three-dimensional theory of SCs.

The procedure for finding the recombination velocity in the SCR using the $J_{SC}(V_{OC})$ or the dark $I-V$ curves is proposed and implemented.

Optimization of the efficiency of silicon SCs depending on the base thickness and the doping level was carried out. Using the example of specific SC,[18] it is demonstrated how photoconversion efficiency can be increased from 26.81% to 27.01% through the proposed optimization.

It was established that in the silicon SCs under consideration, the recombination in the SCR reduces the efficiency of photoconversion by approximately 1%, while the effective lifetime due to this effect decreases by several times. It is also shown that in highly efficient silicon SCs, recombination in the SCR affects key parameters stronger than surface recombination. The results obtained in this work can be used both for the full characterization of highly efficient SCs present today and for the optimization of the key parameters of the next-generation SCs.

We consider the implementation of the proposed theoretical approach in the cmd-PC1D6.2 software[63] or the development of new software tools for its application as promising directions for future research.

ACKNOWLEDGMENTS

This work has been supported by the National Academy of Sciences of Ukraine through budget Program No. III-4-21 of fundamental research. M.E. is grateful to the Natural Sciences and Engineering Research Council of Canada (NSERC) for financial support and to the ACEnet for computational resources.

AUTHOR DECLARATIONS

Conflict of Interest

The authors have no conflicts to disclose.

Author Contributions

V. P. Kostylyov: Conceptualization (equal); Formal analysis (equal); Funding acquisition (equal); Supervision (equal); Writing – review & editing (equal). **A. V. Sachenko:** Conceptualization (equal); Formal analysis (equal); Methodology (equal); Validation (equal); Writing – original draft (equal). **M. Evstigneev:** Formal analysis (equal); Visualization (equal); Writing – review & editing (equal). **I. O. Sokolovskyi:** Data curation (equal); Investigation (equal); Software (equal). **A. I. Shkrebtii:** Data curation (equal); Resources (equal); Writing – review & editing (equal).

DATA AVAILABILITY

The data that support the findings of this study are available from the corresponding author upon reasonable request.

REFERENCES

[1]D. M. Chapin, C. S. Fuller, and G. L. Pearson, "A new silicon p-n junction photocell for converting solar radiation into electrical power," J. Appl. Phys. **25**, 676–677 (1954).
[2]W. Shockley and H. Queisser, "Detailed balance limit of efficiency of p-n junction solar cells," J. Appl. Phys. **32**, 510–519 (1961).
[3]R. M. Swanson, "Approaching the 29% limit efficiency of silicon solar cells," in *Conference Record of the Thirty-first IEEE Photovoltaic Specialists Conference, 2005* (IEEE, 2005), pp. 889–894.
[4]L. C. Andreani, A. Bozzola, P. Kowalczewski, M. Liscidini, and L. Redorici, "Silicon solar cells: Toward the efficiency limits," Adv. Phys.: X **4**, 125–148 (2018).
[5]T. Markvart, "Shockley: Queisser detailed balance limit after 60 years," WIREs Energy Environ. **11**, e430 (2022).

[6]C. Ballif, F.-J. Haug, M. Boccard, P. J. Verlinden, and G. Hahn, "Status and perspectives of crystalline silicon photovoltaics in research and industry," Nat. Rev. Mater. **7**, 597–616 (2022).
[7]T. Tiedje, E. Yablonovitch, G. Cody, and B. Brooks, "Limiting efficiency of silicon solar cells," IEEE Trans. Electron Devices **ED31**, 711–716 (1984).
[8]M. Green, "Limits on the open-circuit voltage and efficiency of silicon solar cells imposed by intrinsic Auger processes," IEEE Trans. Electron Dev. **ED31**, 671–678 (1984).
[9]M. Kerr, A. Cuevas, and P. Campbell, "Limiting efficiency of crystalline silicon solar cells due to coulomb-enhanced Auger recombination," Prog. Photovolt: Res. Appl. **11**, 97–104 (2003).
[10]A. Richter, M. Hermle, and S. Glunz, "Reassessment of the limiting efficiency for crystalline silicon solar cells," IEEE J. Photovolt. **3**, 1184–1191 (2013).
[11]S. Schäfer and R. Brendel, "Accurate calculation of the absorptance enhances efficiency limit of crystalline silicon solar cells with Lambertian light trapping," IEEE J. Photovolt. **8**, 1156–1158 (2018).
[12]A. Sachenko, V. Kostylyov, I. Sokolovsky, and M. Evstigneev, "Effect of temperature on limit photoconversion efficiency in silicon solar cells," IEEE J. Photovolt. **10**, 63–69 (2020).
[13]T. Niewelt, B. Steinhauser, A. Richter, B. Veith-Wolf, A. Fell, B. Hammann, N. Grant, L. Black, J. Tan, A. Youssef, J. Murphy, J. Schmidt, M. Schubert, and S. Glunz, "Reassessment of the intrinsic bulk recombination in crystalline silicon," Sol. Energy Mater. Sol. Cells **235**, 111467 (2022), 1–13.
[14]B. Veith-Wolf, S. Schäfer, R. Brendel, and J. Schmidt, "Reassessment of intrinsic lifetime limit in n-type crystalline silicon and implication on maximum solar cell efficiency," Sol. Energy Mater. Sol. Cells **186**, 194–199 (2018).
[15]D. Engelbrecht and T. Tiedje, "Temperature and intensity dependence of the limiting efficiency of silicon solar cells," IEEE J. Photovolt. **11**, 73–84 (2021).
[16]M. Evstigneev and F. Farahani, "Photon recycling in a solar cell with two Lambertian surfaces," IEEE J. Photovolt. **13**, 260–266 (2023).
[17]Y. Lee, "Beyond the Shockley-Queisser limit: Exploring new frontiers in solar energy harvest," Science **383**, eado4308 (2024).
[18]H. Lin, M. Yang, X. Ru, G. Wang, S. Yin, F. Peng, C. Hong, M. Qu, J. Lu, L. Fang, C. Han, P. Procel, O. Isabella, P. Gao, Z. Li, and X. Xu, "Silicon heterojunction solar cells with up to 26.81 % efficiency achieved by electrically optimized nanocrystalline-silicon hole contact layers," Nat. Energy **8**, 789–799 (2023).
[19]X. Ru, M. Yang, S. Yin, Y. Wang, C. Hong, F. Peng, Y. Yuan, C. Sun, C. Xue, M. Qu, J. Wang, J. Lu, L. Fang, H. Deng, T. Xie, S. (Frank) Liu, Z. Li, and X. Xu, "Silicon heterojunction solar cells achieving 26.6% efficiency on commercial-size p-type silicon wafer," Joule **8**, 1092–1104 (2024).
[20]M. A. Green, E. D. Dunlop, M. Yoshita, N. Kopidakis, K. Bothe, G. Siefer, D. Hinken, M. Rauer, J. Hohl-Ebinger, and X. Hao, "Solar cell efficiency tables (version 64)," Prog. Photovolt.: Res. Appl. **32**, 425–441 (2024).
[21]M. Taguchi, A. Yano, S. Tohoda, K. Matsuyama, Y. Nakamura, T. Nishiwaki, K. Fujita, and E. Maruyama, "24.7% record efficiency HIT solar cell on thin silicon wafer," IEEE J. Photovolt. **4**, 96–99 (2014).
[22]K. Yamamoto, K. Yoshikawa, H. Uzu, and D. Adachi, "High-efficiency heterojunction crystalline Si solar cells," Jpn. J. Appl. Phys. **57**, 08RB20 (2018), 1–8.
[23]J. Nakamura, N. Asano, T. Hieda, C. Okamoto, H. Katayama, and K. Nakamura, "Development of heterojunction back contact Si solar cells," IEEE J. Photovolt. **4**, 1491–1495 (2014).
[24]K. Masuko, M. Shigematsu, T. Hashiguchi, D. Fujishima, M. Kai, N. Yoshimura, T. Yamaguchi, Y. Ichihashi, T. Mishima, N. Matsubara, T. Yamanishi, T. Takahama, M. Taguchi, E. Maruyama, and S. Okamoto, "Achievement of more than 25% conversion efficiency with crystalline silicon heterojunction solar cell," IEEE J. Photovolt. **4**, 1433–1435 (2014).
[25]F. Feldmann, M. Bivour, C. Reichel, M. Hermle, and S. Glunz, "Passivated rear contacts for high-efficiency n-type Si solar cells providing high interface passivation quality and excellent transport characteristics," Sol. Energy Mater. Sol. Cells **120**, 270–274 (2014).
[26]D. Adachi, J. Hernández, and K. Yamamoto, "Impact of carrier recombination on fill factor for large area heterojunction crystalline silicon solar cell with 25.1% efficiency," Appl. Phys. Lett. **107**, 233506 (2015), 1–3.
[27]M. Hermle, F. Feldmann, M. Bivour, J. C. Goldschmidt, and S. W. Glunz, "Passivating contacts and tandem concepts: Approaches for the highest silicon-based solar cell efficiencies," Appl. Phys. Rev. **7**, 021305 (2020).
[28]J. Schmidt, R. Peibst, and R. Brendel, "Surface passivation of crystalline silicon solar cells: Present and future," Sol. Energy Mater. Sol. Cells **187**, 39–54 (2018).
[29]T. Sugiura and N. Nakano, "Transparent conductive oxide materials for bifacial heterojunction back contact solar cells," IEEE Trans. Electron Devices **69**, 3748–3752 (2022).
[30]L. Black and D. Macdonald, "On the quantification of Auger recombination in crystalline silicon," Sol. Energy Mater. Sol. Cells **234**, 11428 (2022), 1–15.
[31]F. Haase, F. Kiefer, S. Schäfer, C. Kruse, J. Krügener, R. Brendel, and R. Peibst, "Interdigitated back contact solar cells with polycrystalline silicon on oxide passivating contacts for both polarities," Jpn. J. Appl. Phys. **56**, 08MB15 (2017), 1–5.
[32]A. Richter, J. Benicka, F. Feldmann, A. Fell, M. Hermle, and S. Glunz, "n-type Si solar cells with passivating electron contact: Identifying sources for efficiency limitations by wafer thickness and resistivity variation," Sol. Energy Mater. Sol. Cells **173**, 96–105 (2017).
[33]P. Altermatt, "Models for numerical device simulations of crystalline silicon solar cells—A review," J. Comput. Electron. **10**, 314–330 (2011).
[34]T. Sugiura and N. Nakano, "Review: Numerical simulation approaches of crystalline-Si photovoltaics," Energy Sci. Eng. **11**, 3888–3906 (2023).
[35]A. Richter, R. Müller, J. Benick, F. Feldmann, B. Steinhauser, C. Reichel, A. Fell, M. Bivour, M. Hermle, and S. W. Glunz, "Design rules for high-efficiency both-sides-contacted silicon solar cells with balanced charge carrier transport and recombination losses," Nat. Energy **6**, 429–438 (2021).
[36]T. Sugiura, S. Matsumoto, and N. Nakano, "Optimization of front diffusion profile in bifacial interdigitated back contact solar cell," IEEE J. Photovolt. **10**, 1582–1590 (2020).
[37]M. Q. Khokhar, H. Yousuf, A. Alamgeer, M. Chu, R. U. Rahman, J. A. Jony, S. Q. Hussain, D. P. Pham, and J. Yi, "Systematic modeling and optimization for high-efficiency interdigitated back-contact crystalline silicon solar cells," Energy Technol. **10**, 2400831 (2024).
[38]A. Fell, K. McIntosh, and K. Fong, "Simplified device simulation of silicon solar cells using a lumped parameter optical model," IEEE J. Photovolt. **6**, 611–616 (2016).
[39]A. Hangleiter, "Nonradiative recombination via deep impurity levels in silicon: Experiment," Phys. Rev. B **35**, 9149–9160 (1987).
[40]A. Hangleiter, "Nonradiative recombination via deep impurity levels in semiconductors: The excitonic Auger mechanism," Phys. Rev. B **37**, 2594–2604 (1988).
[41]J. Szmytkowski, "A simple model of the trap-assisted recombination with the excitonic Auger mechanism," Eur. Phys. J. Plus **135**, 37 (2020), 1–6.
[42]A. Sachenko, V. Kostylyov, V. Vlasyuk, I. Sokolovsky, and M. Evstigneev, "The influence of the exciton nonradiative recombination in silicon on the photoconversion efficiency," in *32 European Photovoltaic Solar Energy Conference and Exhibition* (WIP, 2016), pp. 141–147.
[43]A. Sachenko, V. Kostylyov, and M. Evstigneev, "Space charge region recombination in highly efficient silicon solar cells," Semicond. Phys. Quantum Electron. Optoelectron. **27**, 10–27 (2024).
[44]A. Sachenko, V. Kostylyov, I. Sokolovsky, and M. Evstigneev, "Optimization of textured silicon solar cells," in *47th IEEE Photovoltaic Specialists Conference (PVSC-47)* (IEEE, 2020), pp. 0719–0723.
[45]A. Sachenko, V. Kostylyov, V. Vlasiuk, I. Sokolovskyi, M. Evstigneev, T. Slusar, and V. Chernenko, "Modeling of characteristics of highly efficient textured solar cells based on c-silicon. The influence of recombination in the space charge region," Semicond. Phys. Quantum Electron. Optoelectron. **26**, 5–16 (2023).
[46]K. McIntosh and S. C. Baker-Finch, "A parameterization of light trapping in wafer-based solar cells," IEEE J. Photovolt. **5**, 1563–1570 (2015).

[47]J. Fossum, "Computer-aided numerical analysis of silicon solar cells," Solid State Electron. **19**, 269–277 (1976).
[48]V. Abakumov, V. Perel, and I. Yassievich, *Nonradiative Recombination in Semiconductors* (Amsterdam, Elsevier, 1991).
[49]P. Wurfel, "The chemical potential of radiation," J. Phys. C: Solid State Phys. **15**, 3967 (1982).
[50]A. Schenk, "Finite-temperature full random-phase approximation model of band gap narrowing for silicon device simulation," J. Appl. Phys. **84**, 3684–3695 (1998).
[51]M. Rüdiger, J. Greulich, A. Richter, and M. Hermle, "Parameterization of free carrier absorption in highly doped silicon for solar cells," IEEE Trans. Electron Devices **60**, 2156–2163 (2013).
[52]A. Richter, S. Glunz, F. Werner, J. Schmidt, and A. Cuevas, "Improved quantitative description of Auger recombination in crystalline silicon," Phys. Rev. B **86**, 165202 (2012), 1–14.
[53]S. Dauwe, "Low-temperature surface passivation of crystalline silicon and its application to the rear side of solar cells," Ph.D. thesis (University of Hannover, 2004).
[54]B. Veith-Wolf, "Crystalline silicon surface passivation using aluminum oxide: Fundamental understanding and application to solar cell," Ph.D. thesis (University of Hannover, 2018).
[55]M. Taguchi, H. Sakata, Y. Yoshimine, E. Maruyama, A. Terakawa, M. Tanaka, and S. Kiyama, "An approach for the higher efficiency in the HIT cells," in *IEEE 31st Photovoltaic Specialists Conference* (IEEE, 2005), pp. 866–871.
[56]M. Taguchi, E. Maruyama, and M. Tanaka, "Temperature dependence of amorphous/crystalline silicon heterojunction solar cells," Jpn. J. Appl. Phys. **47**, 814 (2008).
[57]A. Sachenko, V. Kostylyov, V. Vlasiuk, I. Sokolovskyi, M. Evstigneev, A. Shkrebtii, D. Johnston, P. Michael, and T. Missimer, "Characterization and optimization of highly efficient silicon-based textured solar cells: Theory and experiment," in *48th IEEE Photovoltaic Specialists Conference (PVSC-48)* (IEEE, 2021), pp. 0544–0550.
[58]K. Yoshikawa, W. Yoshida, T. Irie, H. Kawasaki, K. Konishi, H. Ishibashi, T. Asatani, D. Adachi, M. Kanematsu, H. Uzu, and K. Yamamoto, "Exceeding conversion efficiency of 26% by heterojunction interdigitated back contact solar cell with thin film Si technology," Sol. Energy Mater. Sol. Cells **173**, 37–42 (2017).
[59]A. Sachenko, V. Kostylyov, V. Vlasiuk, I. Sokolovskyi, and M. Evstigneev, "Analysis of the recombination mechanisms in silicon solar cells with the record 26.6% photoconversion efficiency," in *48th IEEE Photovoltaic Specialists Conference (PVSC-48)* (IEEE, 2021), pp. 0532–0539.
[60]P. Spinelli, B. W. H. van de Loo, A. H. G. Vlooswijk, W. M. M. Kessels, and I. Cesar, "Quantification of pn-junction recombination in interdigitated back-contact crystalline silicon solar cells," IEEE. J. Photovolt. **7**, 1176–1183 (2017).
[61]Q. Su, H. Lin, G. Wang, H. Tang, C. Xue, Z. Li, X. Xu, and P. Gao, "Theoretical limiting-efficiency assessment on advanced crystalline silicon solar cells with Auger ideality factor and wafer thickness modifications," Prog. Photovolt. **32**, 587–598 (2024).
[62]E. Aydin, T. G. Allen, M. D. Bastiani, A. Razzaq, L. Xu, E. Ugur, J. Liu, and S. D. Wolf, "Pathways toward commercial perovskite/silicon tandem photovoltaics," Science **383**, eadh3849 (2024).
[63]H. Haug and J. Greulich, "PC1Dmod 6.2—Improved simulation of c-Si devices with updates on device physics and user interface," Energy Proc. **92**, 60–68 (2016).